ADVANCED ENERGY MATERIALS
www.advenergymat.de

Overcoming Efficiency Limitations of SnS-Based Solar Cells

*Prasert Sinsermsuksakul, Leizhi Sun, Sang Woon Lee, Helen Hejin Park, Sang Bok Kim, Chuanxi Yang, and Roy G. Gordon**

Thin-film solar cells are made by vapor deposition of Earth-abundant materials: tin, zinc, oxygen and sulfur. These solar cells had previously achieved an efficiency of about 2%, less than 1/10 of their theoretical potential. Loss mechanisms are systematically investigated and mitigated in solar cells based on p-type tin monosulfide, SnS, absorber layers combined with n-type zinc oxysulfide, Zn(O,S) layers that selectively transmit electrons, but block holes. Recombination at grain boundaries is reduced by annealing the SnS films in H_2S to form larger grains with fewer grain boundaries. Recombination near the p-SnS/n-Zn(O,S) junction is reduced by inserting a few monolayers of SnO_2 between these layers. Recombination at the junction is also reduced by adjusting the conduction band offset by tuning the composition of the Zn(O,S), and by reducing its free electron concentration with nitrogen doping. The resulting cells have an efficiency over 4.4%, which is more than twice as large as the highest efficiency obtained previously by solar cells using SnS absorber layers.

1. Intoduction

Tin monosulfide (SnS) is a semiconductor material with a band-gap of ≈1.1 eV, which is similar to that of silicon. The optical absorption coefficient of SnS is much larger than that of silicon, so SnS-based solar cells only need to be much thinner than crystalline silicon solar cells. SnS layers less than one micrometer thick can absorb most of the solar spectrum above the band-gap. Charge transport across such thin layers should be relatively immune to defects and impurities compared to silicon, which demands high purity and crystal perfection to make efficient, but expensive, solar cells. The available amounts of tin and sulfur are large enough to supply all of the world's energy. In contrast, the thin-film solar cells based on cadmium telluride (CdTe) and on copper indium gallium sulfide selenide (CIGS) require elements (Te, In, Ga, Se) that are so rare in the Earth's crust that they cannot provide a major amount of solar energy. Copper zinc tin sulfide selenide (CZTS) uses more Earth-abundant elements, but its complex composition complicates its manufacture. SnS, has a much simpler composition, which should allow production by sublimation, similar to the fast and inexpensive way that CdTe cells are made. SnS is stable in the presence of water and oxygen in the atmosphere, where it is found as a mineral, Herzenbergite. Thus SnS has better prospects for long-term stability than organic solar cells and lead iodide perovskites, which are destroyed by oxygen and water. Also, SnS contains only non-toxic elements, whereas other thin-film cells require toxic elements cadmium, tellurium, selenium and/or lead. Although theory predicts that the maximum energy conversion efficiency of single-junction SnS-based solar cells is 32%, existing SnS solar cells has only reached 2% efficiency,[1,2] a value far too low to compete with silicon solar cells with over 20% efficiency.

Here, we systematically examine the causes behind the underperformance of SnS-based solar cells. We demonstrate a logical sequence of five modifications to the fabrication procedure that enabled us to double the efficiency record from 2.04%[1] to 4.36% as certified by NREL. First, SnS films were annealed in hydrogen sulfide to enlarge their crystalline grains and reduce the recombination loss at grain boundaries. Second, the sulfur content of the n-type Zn(O,S) buffer layer was reduced from the value used for as-deposited SnS to form an optimum value for the conduction band offset with the annealed SnS films. Third, the Zn(O,S) films with reduced sulfur content had conductivity too high to form rectifying p-n junctions.[3] Thus the rectifying quality of the junction was restored by adding nitrogen as a dopant to the Zn(O,S) to trap most of its free electrons. Fourth, the open-circuit voltage was increased by passivating the SnS/Zn(O,S):N interface by oxidizing the SnS surface to SnO_2, suppressing recombination centers near the junction. Fifth, the device was further optimized by depositing SnO_2 at the SnS/Zn(O,S):N interface using atomic layer deposition (ALD), to have additional control of the thickness of the SnO_2 layer beyond that provided by oxidation of SnS. The structure of the final device is shown in **Figure 1**, with a schematic diagram and a cross-sectional scanning electron microscopy (SEM) image of an actual device.

Dr. P. Sinermsuksakul, Dr. S. B. Kim, Prof. R. G. Gordon
Department of Chemistry and Chemical Biology
Harvard University
Cambridge, MA, U.S.A
E-mail: gordon@chemistry.harvard.edu
L. Sun, H. H. Park, C. Yang
School of Engineering and Applied Sciences
Harvard University
Cambridge, MA, U.S.A
Prof. S. W. Lee
Department of Physics and Division
of Energy Systems Research
Ajou University
443–749, Suwon, Korea

DOI: 10.1002/aenm.201400496

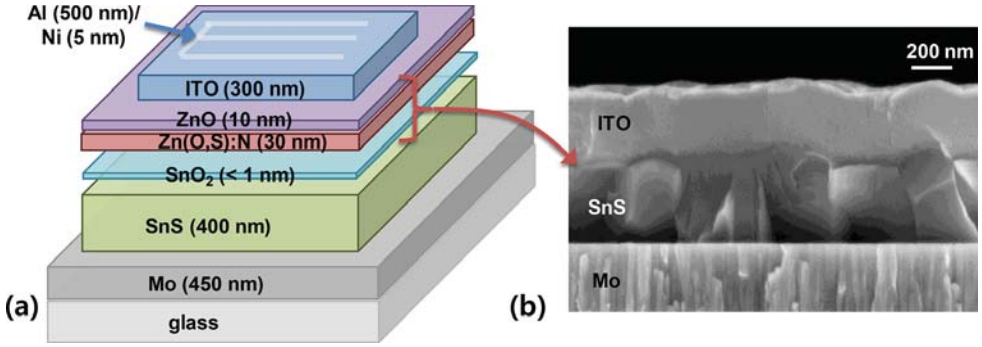

Figure 1. a) A schematic diagram of a SnS-based solar cell and b) a cross-sectional SEM image of an actual cell with SnS annealed in H_2S.

2. Annealing to Reduce Recombination

Post-deposition annealing is frequently used to increase the efficiency of thin film solar cells by improving the material properties of the absorber layer. Annealing can reduce recombination by promoting grain growth and thereby reducing the number of grain boundaries that can catalyze recombination.[4] Annealing can also reduce the number of bulk and interface defects. In the case of SnS, theoretical calculation shows that sulfur vacancies (V_S) have states near the middle of the band gap that could act as recombination catalysts by trapping both holes and electrons.[5,6] Due to the high volatility of sulfur, loss of sulfur from SnS is commonly observed after annealing in an inert atmosphere.[7,8] In this study, SnS films were annealed in a H_2S atmosphere in an attempt to suppress the creation of sulfur vacancies. Comparisons were also made with annealing the films in an inert N_2 atmosphere. Annealing at temperatures above 500 °C for 1 h resulted in an apparent mass loss due to evaporation of SnS from the films. **Figure 2** shows the SEM images of SnS films after annealing in N_2 or H_2S at 400 °C for 1 h. The temperature and annealing atmosphere strongly influence the morphology, crystallinity, and electrical properties of SnS films. The as-deposited SnS films have a nearly columnar microstructure with grain size smaller than the film thickness, along with some smaller grains near to the surface of the substrate (Figure 2a,d). After annealing in N_2, these small grains undergo normal grain growth and produce a more columnar structure (Figure 2e,f). In the presence of a H_2S atmosphere, SnS films also experience abnormal or secondary grain growth[9] (Figure 2c,f) to form much larger grains and fewer grain boundaries. It is evident that a H_2S atmosphere significantly enhances the grain size of SnS compared to N_2.

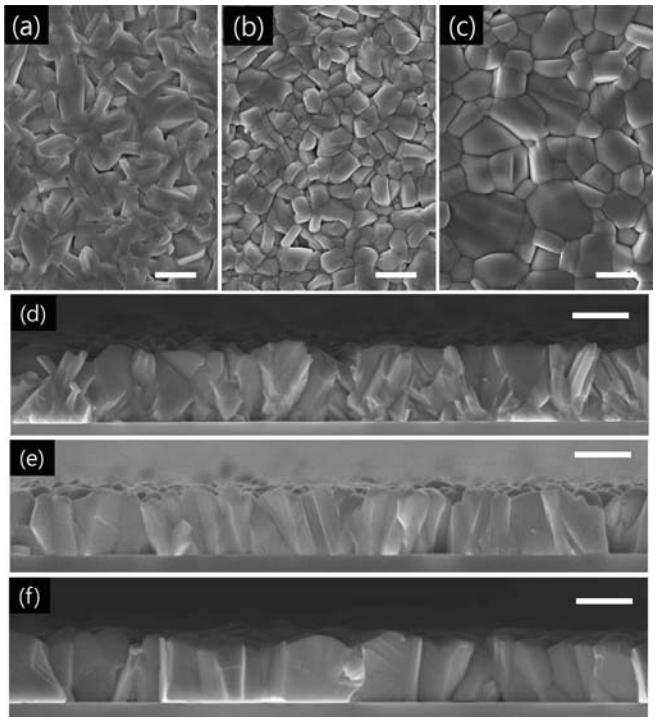

Figure 2. Plane-view and cross sectional SEM images of as-deposited (a,d) and annealed SnS films at 400 °C for 1 h in N_2 (b,e) and H_2S atmospheres (c,f). The scale bars denote 500 nm.

Compared to the as-deposited films, the hole concentration of SnS annealed at 400 °C in H_2S increases roughly by a factor of 3 to 5.7×10^{15} cm^{-3}. The electrical properties of films annealed in a H_2S atmosphere can be found in the Supporting Information (Table S1). The increase in hole concentration might be due to H_2S reducing the number of sulfur vacancies, which can trap the majority-carrier holes. Sulfur vacancies can also catalyze recombination and reduce the minority electron lifetime. Thus H_2S reduction of the number of sulfur vacancies could also have the benefit of increasing the minority liftetime. Thus SnS films (0.4 to 0.5 μm thick) annealed in H_2S at 400 °C for 1 h were used to fabricate the solar cells reported in this study.

3. Optimizing the Conduction Band Offset by Tuning the Composition of Zn(O,S)

For maximum conversion efficiency, heterojunction solar cells often have a "spike" type conduction band offset (CBO), in which the n-type buffer layer has a slightly higher energy at its conduction band minimum than does the p-type absorber layer. This spike CBO minimizes the recombination rate at the p-n junction.[10,11] It is not necessary to have a spike CBO to form an efficient heterojunction solar cell if the recombination velocity at the junction is low enough. High quality CdTe/CdS heterojunctions may function well even with a small negative CBO ("cliff" type). However, our SnS/Zn(O,S) heterojunctions appear to have a high enough recombination velocity that they

perform best with a slightly positive CBO. As long as the size of the positive CBO is kept below 0.4 eV, the photoelectrons generated in the p-type layer can still surmount the small barrier at the junction to be collected in the n-type layer.

For as-deposited 500 nm-thick SnS films, the optimum spike and highest efficiency were obtained by depositing Zn(O,S) with ZnO:ZnS cycle ratio of 6:1, corresponding to a S/Zn ratio of 0.50 based on RBS analysis.[1,12] Using the same S/Zn ratio for Zn(O,S), a device (with an active area of 0.031 cm^2) was made from annealed SnS (H_2S, 400 °C, 1 h) and compared with one using as-deposited SnS (**Figure 3**). These devices were characterized under illumination from a microscope halogen lamp (with a color temperature of 3300 K), which is sufficient to reveal junction characteristics. Based on the double-diode shape (curve (ii) in Figure 3) of the current density–voltage (*J–V*) characteristics, it is evident that the conduction band energy of the annealed SnS is lower than that of as-deposited SnS. Hence a spike that is too large forms at the junction between the annealed SnS and the Zn(O,S) (S/Zn = 0.5), resulting in reduced collection of electrons (Figure S1, Supporting Information).

In order to reduce the conduction band energy of Zn(O,S) to the value needed for an optimum spike at the junction, the sulfur content of the Zn(O,S) was reduced by increasing the ZnO:ZnS cycle ratio from 6:1 to 14:1, corresponding to a decrease of the S/Zn ratio from 0.50 to 0.14. Devices made with these conditions, however, had nearly Ohmic behavior with negligible rectification (Figure 3 and Supporting Information Figure S2). The poor performance of these diodes was traced to the higher conductivity of the Zn(O,S) films with low sulfur content. After decreasing the S/Zn ratio from 0.50 to 0.14, the free electron concentration increases by a factor of 2 to 4.5×10^{19} cm^{-3} and the mobility increases by a factor of 13 to 16.4 cm^2 V^{-1} s^{-1}.

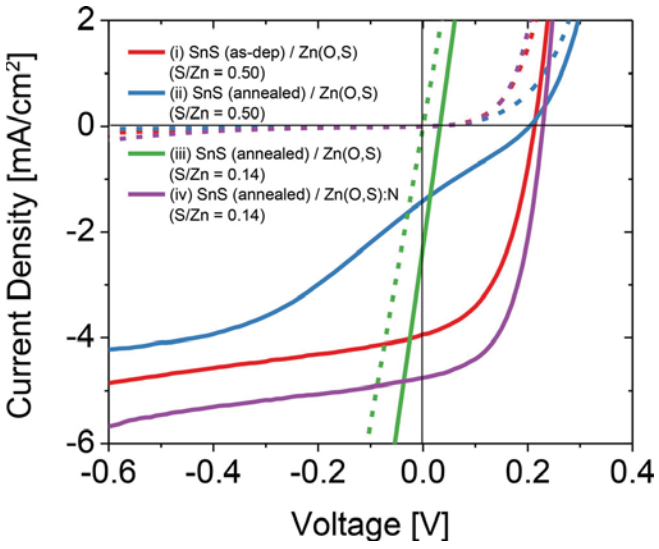

Figure 3. *J–V* characteristics under dark (dashed line) and low illumination (solid line) of devices comprised of i) as-deposited SnS with Zn(O,S) (S/Zn = 0.50), ii) H_2S annealed (400 °C) SnS with Zn(O,S) (S/Zn = 0.50), iii) H_2S annealed (400 °C) SnS with Zn(O,S) (S/Zn = 0.14), and iv) H_2S annealed (400 °C) SnS with nitrogen-doped Zn(O,S):N (S/Zn = 0.14).

4. Improving the Diode Quality by Nitrogen-Doping the Zn(O,S) to Reduce its Carrier Concentration

The diode quality was recovered by doping the Zn(O,S) with nitrogen to trap most of the free electrons and decrease the conductivity. The nitrogen was provided by adding a sub-cycle of diethylzinc and then ammonia gas following each cycle of ZnO in the ALD process. For a ZnO:ZnS cycle ratio of 14:1, the S/Zn ratio is 0.14 and the N/Zn ratio is 0.05 according to RBS analysis. For this composition, the nitrogen doping reduces the electron concentration from 4.5×10^{19} cm^{-3} to 9.3×10^{16} cm^{-3} and the mobility from 16.4 cm^2 V^{-1} s^{-1} to 4.7 cm^2 V^{-1} s^{-1}. The conductivity of the nitrogen-doped Zn(O,S) is reduced by more than three orders of magnitude. The junction made with annealed SnS and the more resistive Zn(O,S):N showed good rectification as shown in Figure 3. Nonetheless, the open-circuit voltage (V_{oc}) and efficiency of these cells were only slightly improved compared to the cells made previously without annealing and nitrogen doping (**Table 1**). This suggests that significant recombination pathways remained in these cells.

5. Oxidation of the SnS/Zn(O,S):N Interface

For SnS-based solar cells, the conversion efficiency is mainly limited by the relatively low open-circuit voltage (V_{oc} < 0.25 V, J_{sc} ≥ 19 mA cm^{-2}).[1,2,13] The authors discovered that oxidizing the SnS surface could increase the cell voltage significantly. Several oxidation treatments of the SnS films were carried out, including an ambient air exposure at room temperature for 1 day, annealing in 10 Torr of air at 200 °C for 30 min, and an exposure to 7.5 Torr s of H_2O_2 vapor at 120 °C. The thicknesses of SnO_2 made by these oxidation treatments were estimated by X-ray photoelectron spectroscopy (XPS) analysis (Table 1). The open-circuit voltage of these devices increased significantly from a typical value of 0.25 V to above 0.35 V (**Figure 4** and Table 1). Fill factor and current were also improved. Evidently, only a few monolayers of SnO_2 greatly reduced the recombination loss at the SnS/Zn(O,S) interface.

The device with SnO_2 formed by an exposure to H_2O_2 was characterized independently at the National Renewable Energy Laboratory (NREL), showing cell performance characteristics of short-circuit current (J_{sc}) = 20.2 mA cm^{-2}, open-circuit voltage (V_{oc}) = 0.372 V, fill factor (*FF*) = 58.0%, and efficiency (η) = 4.36% as shown in **Figure 5**. This device has the highest recorded and independently verified efficiency of any SnS-based solar cell to date.

6. ALD of SnO_2 at the SnS/Zn(O,S):N interface

For the aforementioned devices, the oxidized tin atoms were contributed by the SnS layer. In order to provide a more controllable amount of tin oxide, a previously reported ALD process was used for the deposition of SnO_2,[14] in which doses of a cyclic tin amide precursor were alternated with doses of H_2O_2 vapor at 120 °C. Devices with 5 and 10 ALD cycles of SnO_2 were fabricated to examine the effect of thickness on device

Table 1. Summary of device performance characterisitcs with various passivation treatments. The device area is 0.24 cm^2. The device with an exposure to H_2O_2 was characterized indenpdently at NREL.

SnO_2 growth methods	Temp. [°C]	Conditions	SnO_2 thickness [nm]	J_{sc} [mA cm^{-2}]	V_{oc} [V]	FF	Eff. [%]
No SnO_2	N/A	N/A	0.0	18.7	0.26	0.51	2.50
Air	R.T.	24 h	≈0.4	19.3	0.36	0.53	3.70
	200	10 Torr 30 min	≈0.6	21.6	0.35	0.58	4.36
H_2O_2	120	7.5 Torr s (5 cycles)	0.5–0.6	22.7	0.37	0.54	4.54
H_2O_2 (NREL)	120	7.5 Torr s (5 cycles)	0.5–0.6	20.2	0.37	0.58	4.36
ALD	120	5 cycles	0.6–0.7	22.6	0.39	0.53	4.63
	120	10 cycles	0.9–1	21.5	0.31	0.43	3.07

performance. As shown in **Figure 6**, the device with 5 ALD cycles (0.6 nm) of SnO_2 demonstrated higher performance than the one with 10 ALD cycles (1.0 nm). Compared to the earlier device with an exposure to 7.5 Torr s of H_2O_2 vapor, the device with 5 ALD cycles of SnO_2 increased V_{oc} from 0.37 to 0.39 V and efficiency from 4.54% to 4.63%.

The three best-performing devices have the SnO_2 layer deposited or formed by 5 ALD cycles at 120 °C, an exposure to 7.5 Torr s of H_2O_2 vapor at 120 °C, and annealing in 10 Torr of air at 120 °C for 30 min, respectively. The external quantum efficiency was measured in the dark for the three devices (**Figure 7**a). The internal quantum efficiency was derived from the external quantum efficiency by correcting for the reflection spectrum of each device (Figure 7b). The external quantum efficiency is only moderately lower than the internal counterpart, indicating that photon absorption is reasonably high in the device. The peak of the internal quantum efficiency is over 90% but the yield drops to under 30% in the near infrared range (800–1000 nm), in which the optical absorption coefficient is lower. Less complete absorption of photons and loss of photoelectrons by recombination both contribute to the reduced infrared yield. Photon absorption may be increased by growing thicker SnS films and increasing the high-angle reflectivity of the back contact via texturing and nanostructuring.

The amount of SnO_2 deposited or formed on the SnS surface was measured by XPS. **Figure 8**a shows the XPS spectra of Sn 3d peak for as-deposited and annealed (400 °C in H_2S) pure SnS films, indicating that both films are free of oxygen contamination. The position of SnS 3d peak (485.8 eV) is consistent with the literature value.[11] Figure 8b shows the XPS spectra of Sn 3d peak for SnS(annealed)/SnO_2 heterostructures with various passivation treatments. A thin passivation layer with merely a few monolayers of SnO_2 (0.6–0.7 nm) yields the highest efficiency, while the improvement diminishes with a thicker SnO_2 layer. This result is expected since SnO_2 is not a suitable n-type buffer layer for SnS. SnS/SnO_2 solar cells were

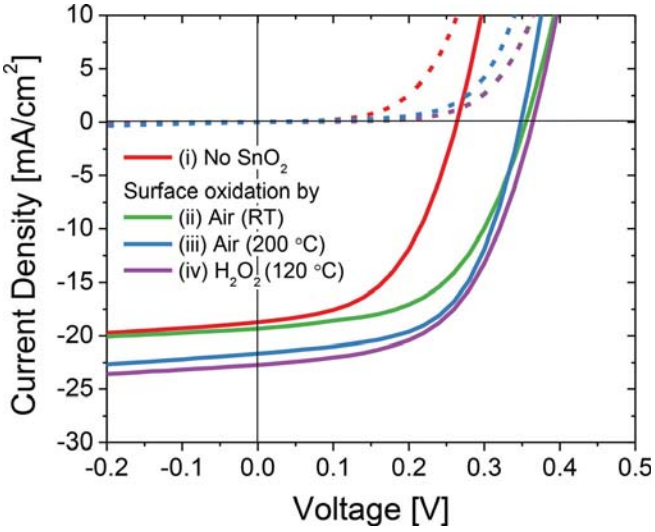

Figure 4. *J–V* curves under dark (dashed line) and AM1.5G, 100 mW cm^{-2} illumination (solid line) for devices comprised of H_2S annealed SnS with Zn(O,S):N (S/Zn = 0.14) i) in the absence of a SnO_2 layer, or with a SnO_2 layer formed by oxidizing the SnS surface (after annealing in H_2S but before Zn(O,S):N deposition) via ii) an ambient air exposure at room temperature for 1 day, iii) annealing in 10 Torr of air at 200 °C for 30 min, and iv) an exposure to 7.5 Torr s of H_2O_2 vapor at 120 °C.

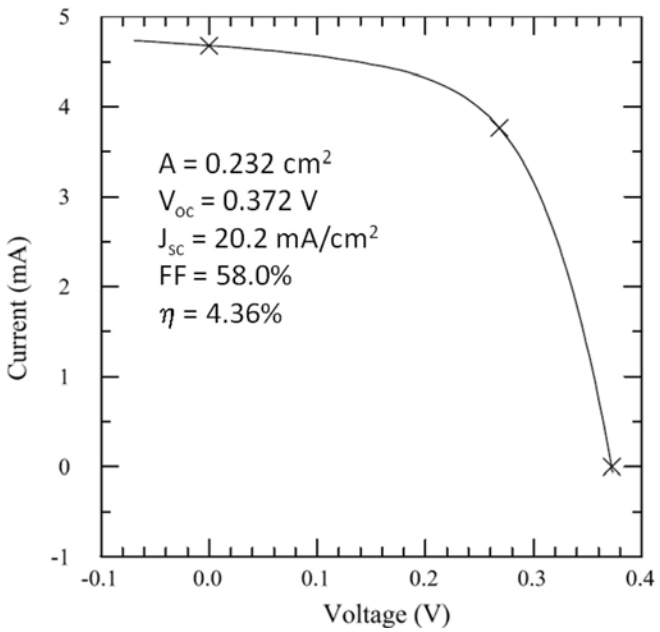

Figure 5. *J–V* characteristics of the champion device with a record efficiency of 4.36%, certified by NREL.

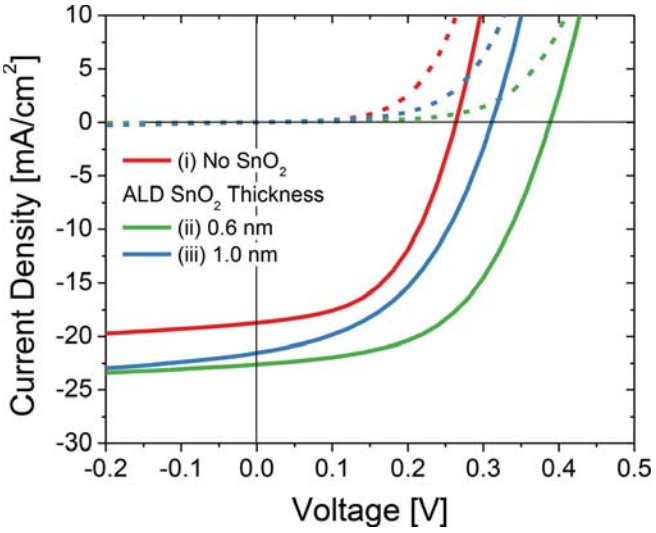

Figure 6. *J–V* curves under dark (dashed line) and AM1.5G, 100 mW cm^{-2} illumination (solid line) for devices comprised of H_2S annealed SnS with Zn(O,S):N (S/Zn = 0.14) i) in the absence of a SnO_2 layer, and with an ALD SnO_2 layer with a thickness of ii) 0.6 nm and iii) 1.0 nm. A few monolayers (0.6 nm) of SnO_2 yield the highest efficiency, while the improvement diminishes with a thicker (1.0 nm) SnO_2 layer.

reported to have very low V_{oc} in the range of 40–90 mV.[15] Once the SnO_2 layer becomes thick enough to form a conduction band, the optimum SnS/Zn(O,S):N spike will be replaced by an undesired SnS/SnO_2 cliff with reduced efficiency.[16]

Three possible mechanisms could explain why a layer of SnO_2 could improve device performance. One mechanism is that the SnO_2 layer serves as a diffusion barrier that prevents zinc diffusion from Zn(O,S):N into SnS. Theoretical studies show that zinc can substitute into tin sites in SnS with relatively low energy input.[6] The zinc impurities (Zn_{Sn}) are calculated to have mid-gap energy levels that could act as recombination centers in SnS. This is supported by our observation that SnS/Zn(O,S):N junctions degrade rapidly when heated to temperatures above 250 °C, losing their rectification and becoming Ohmic. The Ohmic behavior might be caused by increased diffusion of zinc into SnS at higher temperatures, resulting in a significant increase in recombination near the junction. Another mechanism is that the SnO_2 layer serves as a diffusion barrier that limits sulfur diffusion out of SnS during the deposition of Zn(O,S). It is known that heating SnS in vacuum results in loss of sulfur.[17] Theoretical studies predict that sulfur vacancies (V_S) also have mid-gap energy levels that could act as recombination centers in SnS.[4] A third possible mechanism is that oxygen reacts with the surface of the SnS and passivates trap states on and between adjacent grains. This third mechanism is supported by theoretical calculations stimulated by our experimental results showing that oxygen exposure improves SnS solar cells.[18] Further study is needed to understand more fully the mechanisms by which oxygen improves their performance.

7. Conclusion

In conclusion, we enhanced SnS-based solar cells to a record high efficiency of 4.36% by a logical sequence of five modifications to the fabrication procedure. SnS was annealed to enlarge the crystalline grains, thereby increasing the mobility of carriers and reducing the number of grain boundaries that catalyze recombination. The conduction band minimum of Zn(O,S) was lowered by reducing the sulfur content to form an optimum spike with the annealed SnS. The carrier concentration of the oxygen-rich Zn(O,S) was reduced by nitrogen doping to restore the diode quality. Recombination across the junction was reduced by inserting a few monolayers of SnO_2 between SnS and Zn(O,S):N. Reduced recombination increased the cell voltage and enhanced the efficiency to a record high over 4.36% for SnS-based solar cells. Further improvement in efficiency may require enhancing the quality of bulk SnS and suppressing recombination at the junction and grain boundaries. Efficiency may also be enhanced by growing thicker SnS films, increasing the reflectivity of the back contact, and reducing the contact resistance and recombination loss at the back contact.

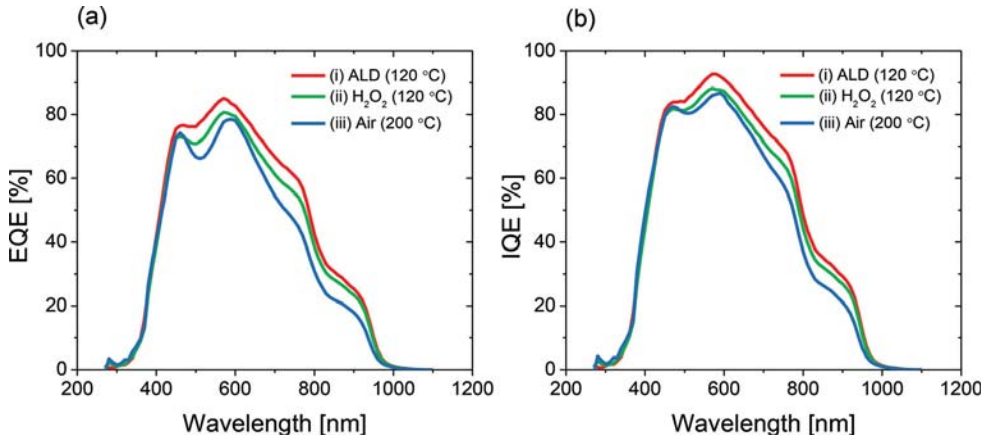

Figure 7. a) External quantum efficiency (EQE) and b) internal quantum efficiency (IQE) for devices with a SnO_2 layer formed via i) 5 cycles of ALD at 120 °C, ii) an exposure to 5 cycles of 7.5 Torr s H_2O_2 vapor at 120 °C, and iii) annealing in 10 Torr of air at 200 °C for 30 min.

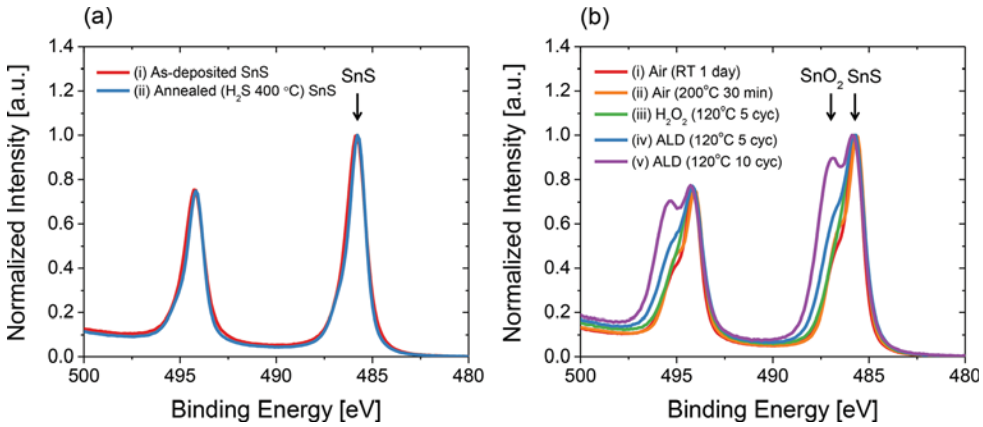

Figure 8. Normalized XPS spectra (Sn 3d) of a-i) as-deposited and a-ii) annealed SnS films (400 °C in H_2S) and b) annealed SnS films (400 °C in H_2S) with a SnO_2 layer formed via b-i) an ambient air exposure at room temperature for 1 day, b-ii) annealing in 10 Torr of air at 200 °C for 30 min, b-iii) an exposure to 5 cycles of 7.5 Torr s H_2O_2 vapor at 120 °C, and b-iv) 5 and b-v) 10 cycles of ALD at 120 °C, respectively.

8. Experimental Section

Solar Cell Fabrication: The solar cells were deposited on glass substrates coated with molybdenum metal by RF sputtering (columnar structure of Mo in Figure 1b).[19] The Mo film has thickness of 0.45 μm and sheet resistance of 0.30 Ohm/square. The SnS films (0.4–0.5 μm) were deposited at 200°C by ALD using alternating doses of tin precursor vapor and a gas mixture of 4% H_2S in N_2.[20] The tin precursor, bis(*N,N'*-diisopropylacetamidinato)tin(II), $Sn(CH_3C(N^iPr)_2)_2$,[20] was sublimed from its solid state in a bubbler at 90 °C. Nitrogen gas at approximately 5 Torr was introduced into the head space of the bubbler to assist in transporting precursor vapor to the custom-built tubular ALD reactor. Three doses of tin amidinate precursor supplied a total exposure of 1.5 Torr s during each cycle. After purging the reactor with flowing N_2 for 3 s, a gas mixture of 4% H_2S in N_2 (Airgas Inc.) provided a H_2S exposure of 1.2 Torr s to form SnS. This process deposits 0.88 Å of SnS during each ALD cycle. Annealing of SnS films was carried out in the same reactor chamber with 10 Torr of pure H_2S (Matheson Tri-gas) or N_2 for 1 h at various temperatures up to 400 °C. To form tin oxide (SnO_2), oxidation of the SnS surface was carried out by several methods, including an ambient air exposure at room temperature for 1 day, annealing in 10 Torr of air at 200 °C for 30 min, and an exposure to a total of 7.5 Torr s of hydrogen peroxide vapor (H_2O_2) in the ALD chamber at 120 °C, dosed in 5 cycles of 1.5 Torr s each. Alternatively, SnO_2 was deposited by ALD using a cyclic tin amide precursor and H_2O_2 at 120 °C for various numbers of cycles.[14] Zn(O,S) (30 nm) and ZnO (10 nm) were then deposited by ALD using diethyl zinc (DEZ), H_2O and a gas mixture of 4% H_2S in N_2 (Airgas Inc). Nitrogen-doped Zn(O,S) was deposited by ALD using a cycle sequence of $[DEZ\text{-}H_2O\text{-}DEZ\text{-}NH_3]_x$-$[DEZ\text{-}H_2S]_1$ with 10 seconds of N_2 purge between each dose of vapor. The exposure of ammonia was approximately 11 Torr s. An undoped ZnO layer (10 nm) was deposited by 50 ALD cycles of DEZ-H_2O. This ZnO layer may protect the underlying layers from being damaged by subsequent RF sputtering of indium tin oxide (ITO). The device active area was defined to be either 0.03 or 0.24 cm^2 by patterned ITO (300 nm) deposited by RF sputtering through a shadow mask. For devices with an active area of 0.24 cm^2, the devices were completed by depositing contact metal grid lines of Ni (5 nm)/Al (500 nm) by electron beam evaporation.

Characterization: Device morphology was examined with field-emission scanning electron microscopy (FESEM, Zeiss, Ultra-55). Rutherford backscattering spectrometry (RBS, Ionex 1.7 MV Tandetron) was used to determine the elemental composition of Zn(O,S) and nitrogen-doped Zn(O,S). The electrical properties of films were determined by Hall measurements (K2500, MMR Technologies) using the Van der Pauw method with Au or In contacts. For cells with an active area of 0.03 cm^2, the *J–V* characteristics was measured under the illumination from a microscope halogen lamp (color temperature = 3300 K) to test the junction behavior. For devices with an active area of 0.24 cm^2, *J–V* characteristics were measured by Agilent 4156C and Keithley 2400 semiconductor characterization systems with standard 100 mW cm^{-2} AM 1.5G illumination. The standard 1-sun illumination was generated by a Newport Oriel 91194 solar simulator with a 1600 W ozone-free Xe-lamp with an AM1.5G filter and a Newport Oriel 6895 f1ux controller calibrated by an NREL-certified Si reference cell equipped with a BG-39 window. Quantum efficiency measurements were made using a PV Measurements QEX7 tool.

Supporting Information

Supporting Information is available from the Wiley Online Library or from the author.

Acknowledgements

P.S., L.S., and S.W.L. contributed equally to this work. The authors thank Tonio Buonassisi, Katy Hartman, Vera Steinmann, and Riley Brandt at MIT for their help with *J–V* and EQE measurements and Paul Ciszek at NREL for testing and certifying the devices. The authors thank Yun Seog Lee at MIT for providing device shadow masks. This work was supported in part by the U.S. Department of Energy SunShot Initiative under Contract No. DE-EE0005329. This work was performed in part at the Center for Nanoscale Systems (CNS), a member of the National Nanotechnology Infrastructure Network (NNIN), supported by the National Science Foundation under NSF award No. ECS-0335765.

Received: March 21, 2014
Revised: May 23, 2014
Published online:

[1] P. Sinsermsuksakul, K. Hartman, S. B. Kim, J. Heo, L. Sun, H. H. Park, R. Chakraborty, T. Buonassisi, R. G. Gordon, *Appl. Phys. Lett.* **2013**, *102*, 053901.
[2] T. Ikuno, R. Suzuki, K. Kitazumi, N. Takahashi, N. Kato, K. Higuchi, *Appl. Phys. Lett.* **2013**, *102*, 193901.
[3] H. H. Park, R. Heasley, R. G. Gordon, *Appl. Phys. Lett.* **2013**, *102*, 132110.

[4] H. H. Park, R. Heasley, L. Sun, V. Steinmann, R. Jaramillo, K. Hartman, R. Chakraborty, P. Sinsermsuksakul, D. Chua, T. Buonassisi, R. G. Gordon, *Prog. Photovoltaics* **2014**, DOI:10.1002/pip.2504.
[5] J. Vidal, S. Lany, M. d'Avezac, A. Zunger, A. Zakutayev, J. Francis, J. Tate, *Appl. Phys. Lett.* **2012**, *100*, 032104.
[6] B. D. Malone, E. Kaxiras, *unpublished* **2013**.
[7] M. Devika, N. K. Reddy, S. V. Reddy, K. Ramesh, K. R. Gunasekhar, *J. Mater. Sci. Mater. Electron.* **2009**, *20*, 1129.
[8] B. Ghosh, R. Bhattacharjee, P. Banerjee, S. Das, *Appl. Surf. Sci.* **2011**, *257*, 3670.
[9] C. V. Thompson, *Ann. Rev. Mater. Sci.* **1990**, *20*, 245.
[10] A. Niemegeers, M. Burgelman, A. Devos, *Appl. Phys. Lett.* **1995**, *67*, 843.
[11] T. Minemoto, T. Matsui, H. Takakura, Y. Hamakawa, T. Negami, Y. Hashimoto, T. Uenoyama, M. Kitagawa, *Sol. Energy Mater. Sol. Cells* **2001**, *67*, 83.
[12] L. Sun, R. Haight, P. Sinsermsuksakul, S. B. Kim, H. H. Park, R. G. Gordon, *Appl. Phys. Lett.* **2013**, *103*, 181904.
[13] A. Schneikart, H. J. Schimper, A. Klein, W. Jaegermann, *J. Phys. D Appl. Phys.* **2013**, *46*, 305109.
[14] J. Heo, A. S. Hock, R. G. Gordon, *Chem. Mater.* **2010**, *22*, 4964.
[15] J. J. M. Vequizo, M. Ichimura, *Japan. J. Appl. Phys.* **2012**, *51*, 38.
[16] M. Sugiyama, K. T. R. Reddy, N. Revathi, Y. Shimamoto, Y. Murata, *Thin Solid Films* **2011**, *519*, 7429.
[17] M. Devika, N. K. Reddy, K. Ramesh, K. R. Gunasekhar, E. S. R. Gopal, K. T. R. Reddy, *Semicond. Sci. Technol.* **2006**, *21*, 1125.
[18] G. A. Tritsaris, B. D. Malone, E. Kaxiras, *J. Appl. Phys.* **2014**, *115*, 173702.
[19] J. H. Scofield, A. Duda, D. Albin, B. L. Ballard, P. K. Predecki, *Thin Solid Films* **1995**, *260*, 26.
[20] P. Sinsermsuksakul, J. Heo, W. Noh, A. S. Hock, R. G. Gordon, *Adv. Energy Mater.* **2011**, *1*, 1116.

